Dynamic Chirality: Keen Selection in the Face of Stereochemical Diversity in Mechanically Bonded Compounds**

Hsian-Rong Tseng,[a] Scott A. Vignon,[a] Paul C. Celestre,[a] J. Fraser Stoddart,*[a] Andrew J. P. White,[b] and David J. Williams*[b]

Dedicated to Professor Ernest L. Eliel on the occasion of his 80th birthday

Abstract: The template-directed syntheses, employing bisparaphenylene-[34]crown-10 (BPP34C10), 1,5-dinaphthoparaphenylene-[36]crown-10 (1/5NPPP36C10), and 1,5-dinaphtho-[38]crown-10 (1/5DNP38C10) as templates, of three [2]catenanes, whereby one of the two bipyridinium units in cyclobis(paraquat-*p*-phenylene) is replaced by a bipicolinium unit, are described. The crude reaction mixtures comprising the [2]catenanes all contain slightly more of the homologous [3]catenanes, wherein a "dimeric" octacationic cyclophane has the crown ether macrocycles encircling the alternating bipyridinium units with the bipicolinium units completely unfettered. X-ray crystallography, performed on all three [2]catenanes and two of the three [3]catenanes reveals co-conformational and stereochemical preferences that are stark and pronounced. Both the [3]catenanes crystallize as mixtures of diastereoisomers on account of the axial chirality associated with the picolinium units in the solid state. Dynamic ^{1}H NMR spectroscopy is employed to probe in solution the relative energy barriers for rotations by the phenylene and pyridinium rings in the tetracationic cyclophane component of the [2]catenanes. Where there are co-conformational changes that are stereochemically "allowed", crown ether circumrotation and rocking processes are also investigated for the relative rates of their occurrence. The outcome is one whereby the three [2]catenanes containing BPP34C10, 1/5NPPP36C10, and 1/5DNP38C10 exist as one major enantiomeric pair of diastereoisomers amongst two, four, and eight diastereoisomeric pairs of enantiomers, respectively. The diastereoisomerism is a consequence of the presence of axial chirality together with helical and/or planar chirality in the same interlocked molecule. These [2]catenanes constitute a rich reserve of new stereochemical types that might be tapped for their switching and mechanical properties.

Keywords: chirality · NMR spectroscopy · stereochemistry · structure elucidation · supramolecular chemistry

Introduction

During the past 15 years, certain molecular recognition-based, self-assembly protocols, which have been pioneered by us,[1] have been employed in the template-directed synthesis[2] of oligocatenanes, which include among others olympiadane[3] and a branched [7]catenane.[4] In addition to incorporating crown ether templates with π-electron-rich aromatic ring systems, these exotic molecules have captured within themselves two different tetracationic cyclophanes, one, a centrally positioned cyclobis(paraquat-4,4′-biphenylene),[5] and the other peripherally located cyclobis(paraquat-*p*-phenylene)s,[6] both containing a pair of π-electron-deficient bipyridinium units. These highly ordered interlocked molecules owe their formation and precise intercomponent geometries to three different kinds of noncovalent interactions: 1) C–H···O interactions[7] between the hydrogen atoms on the encircled bipyridinium units and the centrally located oxygen atoms in the polyether loops of the crown ethers, 2) π···π stacking interactions[8] between electron-donating dioxybenzene or dioxynaphthalene ring systems and the electron-accepting bipyridinium units, and 3) C–H···π interactions[9] between appropriately oriented hydrogen atoms on the encircled π-electron-rich aromatic rings and the faces of the bridging bitolyl and xylyl spacers in the tetracationic cyclophanes. In

[a] Prof. J. F. Stoddart, Dr. H.-R. Tseng, S. A. Vignon, P. C. Celestre
Department of Chemistry and Biochemistry
University of California, Los Angeles
405 Hilgard Avenue, Los Angeles, CA 90095-1569 (USA)
Fax: (+1) 310 206-1843
E-mail: stoddart@chem.ucla.edu

[b] Prof. D. J. Williams, Dr. A. J. P. White
Chemical Crystallography Laboratory
Department of Chemistry, Imperial College
South Kensington, London, SW7 2AY (UK)
Fax: (+44) 207-594-5835

[**] "Molecular Meccano", Part 66. For Part 65, see: S.-H. Chiu, S. J. Rowan, S. J. Cantrill, J. F. Stoddart, D. J. Williams, *Chem. Eur. J.* **2002**, *8*, 5170–5183.

  0947-6539/03/0902-0543 $ 20.00+.50/0

the case of the much simpler [2]catenane homologues, replacement of one of the two bipyridinium units with either a bis(pyridinium)ethylene[10] or diazapyrenium[11] unit results in the production of nondegenerate interlocked molecules. In such [2]catenanes, we have demonstrated[10, 11] that the crown ether components can be moved between the two distinct recognition sites in the constitutionally unsymmetrical cyclophanes either chemically or electrochemically. This kind of mechanical switching introduces the possibility of using these [2]catenanes as controllable, bistable molecular switches.[12–14] Related mechanical movements between the two macrocyclic components of [2]catenanes, in which the degeneracy has been removed from the crown ether by having both tetrathiafulvalene and 1,5-dioxynaphthalene ring systems incorporated as electron donors, can be stimulated electrically in the setting of solid-state devices.[15] Indeed, electronically reconfigurable, bistable memory devices have been developed[16] by sandwiching such switchable [2]catenanes as monolayers between Ti/Al and polysilicon electrodes.

Following another line of reasoning for the construction of artificial molecular machinery,[17] we have recently synthesized and characterized a molecular-level abacus based on a [2]rotaxane that can be operated both electrochemically and photochemically.[18] In this particular [2]rotaxane, the dumbbell-shaped component is endowed with a photoactive stopper at one end and a slippage stopper,[19] with reference to a tailored ring component, for example, bisparaphenylene[34]crown-10 (BPP34C10), at its other end. The thermodynamically controlled assembly of the rotaxane was achieved with the aid of two π-electron-deficient recognition sites, provided by bipyridinium and bipicolinium units, for matching with two π-electron-rich hydroquinone rings in BPP34C10. Spectroscopic studies, along with electrochemical investigations, indicated that the stable translational isomer is the one with the BPP34C10 ring encircling the sterically and electronically more attractive planar bipyridinium unit rather than the nonplanar bipicolinium one. Photoinduced electron transfer from the photoactive stopper to the bipyridinium unit, which possesses the lower reduction potential, destabilizes its noncovalent bonding interactions with BPP34C10. In the presence of a sacrificial electron donor to reduce the incipiently oxidized stopper, this destabilization results in the BPP34C10 ring being displaced from the bipyridinium unit to the bipicolinium unit. This research demonstrated the ease with which a bistable molecular switch can be assembled in a modular fashion using a collection of readily available building blocks.

In a parallel set of experiments, we have been exploring the consequences of replacing one of the bipyridinium units in the cyclobis(paraquat-*p*-phenylene) component of the donor/acceptor catenanes with a bipicolinium unit. In addition to BPP34C10, we have employed the crown ethers, 1,5-dinaphtho[38]crown-10[20] (1/5DNP38C10) and 1,5-naphthoparaphenylene[36]crown-10[21] (1/5NPPP36C10) as templates to be mechanically interlocked by the modified, nondegenerate tetracationic cyclophane. Here, we report on 1) the synthesis, with BPP34C10, 1/5NPPP36C10, and 1/5DNP38C10 as the templates, of three [2]catenanes where the tetracationic cyclophane component contains both a bipyridinium and a bipicolinium unit, and the 'homologous' [3]catenanes incorporating the 'dimeric' octacationic cyclophane with doubly alternating bipyridinium and bipicolinium units; 2) the solid-state structures of all the [2]catenanes and two of the [3]catenanes; 3) the nature of the relative ring movements with respect to each other in the three [2]catenanes as probed by dynamic ^{1}H NMR spectroscopy in solution; and 4) a detailed investigation of the stereochemistry of the [2]catenanes. These investigations mark the first important steps in the construction and evaluation of the potential of such mechanically interlocked molecules to act as switches in solution, prior to their incorporation into solid-state devices.

Results and Discussion

Synthesis: The catenanes were assembled (Scheme 1) by using conventional reaction conditions,[10, 11] wherein the crown ethers serve in turn as templates for the formation of the tetracationic and octacationic cyclophanes to give the [2]- and [3]catenanes, respectively. The reaction of the dibromide

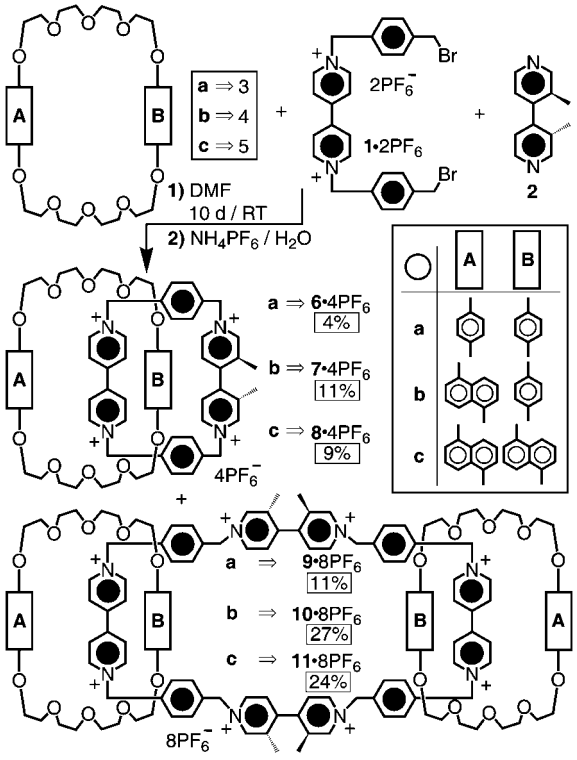

Scheme 1. The template-directed synthesis of the [2]catenanes **6**·4PF$_6$, **7**·4PF$_6$, and **8**·4PF$_6$, and of the [3]catenanes **9**·8PF$_6$, **10**·8PF$_6$, and **11**·8PF$_6$.

salt[6] **1**·2PF$_6$ with bipicoline (**2**) in turn with the crown ethers **3** (BPP34C10), **4** (1/5NPPP36C10), and **5** (1/5DNP38C10) afforded the [2]catenanes **6**·4PF$_6$, **7**·4PF$_6$, and **8**·4PF$_6$, respectively, in yields of 4, 11, and 9%. In addition, the [3]catenanes **9**·8PF$_6$, **10**·8PF$_6$, and **11**·8PF$_6$ were isolated in yields of 11, 27, and 24%, respectively. It should be noted that the [3]catenanes were obtained as the major catenated products in all three reactions.

0947-6539/03/0902-0544 $ 20.00+.50/0 *Chem. Eur. J.* **2003**, *9*, No. 2

X-ray structural analysis: Single crystals, suitable for X-ray crystallography, of five of the six catenanes were grown using the vapor diffusion technique. In the case of the three catenanes **6**·4PF$_6$, **7**·4PF$_6$ and **8**·4PF$_6$, *i*Pr$_2$O was allowed to diffuse into a solution of the compounds in MeCN. In the case of the two [3]catenanes **9**·8PF$_6$ and **11**·8PF$_6$, *t*BuOMe was used as the diffusing solvent in place of *i*Pr$_2$O. Sometimes, a few drops of an aromatic solvent (PhH and/or PhMe) were added to the MeCN solutions to facilitate crystallizations. One of the [3]catenanes, namely **10**·8PF$_6$, did not form single crystals that were suitable for X-ray structural analysis.

The [2]catenane **6**$^{4+}$ has crystallographic C_2 symmetry about an axis passing through the centers of the linking C–C bonds of the bipyridinium and bipicolinium units in the solid-state (Figure 1). The *O*-methylene groups of both hydroquinone

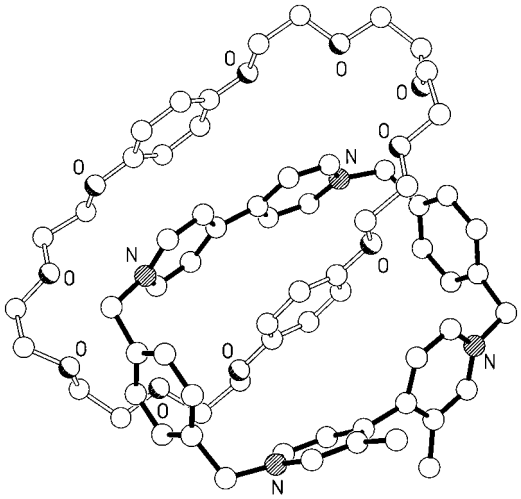

Figure 1. The solid-state structure of the [2]catenane **6**$^{4+}$. The C–H$\cdots\pi$ interaction between the inside hydroquinone ring and one of the paraxylyl rings has H$\cdots\pi$, 2.80 Å; C–H$\cdots\pi$, 161°. The C–H$\cdots$O hydrogen bond between the lowermost α-CH-bipy hydrogen atom and the central oxygen atom of the lower polyether loops has C$\cdots$O, H$\cdots$O, 3.33, 2.41 Å; C–H$\cdots$O, 161°.

rings have anti geometries. The torsional twists of the inside bipyridinium and outside bipicolinium units are 7 and 59°, respectively. The mean interplanar separations between the inside hydroquinone ring and the centers of the outside bipicolinium and inside bipyridinium units are 3.95 and 3.38 Å, respectively: the separation between the outside hydroquinone ring and the inside bipyridinium unit is 3.40 Å. The [2]catenane co-conformation is stabilized by the normal combination of $\pi\cdots\pi$, C–H$\cdots\pi$, and C–H$\cdots$O interactions. The packing of the [2]catenane molecules is controlled predominantly by van der Waals forces, as there is no $\pi-\pi$ stacking that extends beyond the molecule.

In the solid-state (Figure 2), the structure of the [2]catenane **7**$^{4+}$ has only approximate C_2 symmetry and has the 1,5-dioxynaphthalene ring system located outside, whereas the hydroquinone ring is positioned inside the tetracationic cyclophane. There are substantial differences in the twist angles within the bipyridinium and bipicolinium units; these are 2 and 61°, respectively. The mean interplanar separations between the inside hydroquinone ring and the inside bipyridinium and outside bipicolinium units are 3.46 and 3.92 Å, respectively: the separation between the outside 1,5-dioxynaphthalene ring system and the inside bipyridinium unit is 3.45 Å. Once again, stabilization of the [2]catenane co-conformation is achieved by complementary $\pi\cdots\pi$, C–H$\cdots\pi$, and C–H$\cdots$O interactions. The [2]catenane molecules pack in the crystal to form polar π-stacked tapes (Figure 3), the outside 1,5-dihydroxynaphthalene ring system of one molecule being aligned parallel with one of the paraxylyl units of the next. The mean interplanar separation of the extended π-systems is 3.44 Å. The outer edges of the tapes are populated by the methyl substituent of the bipicolinium units.

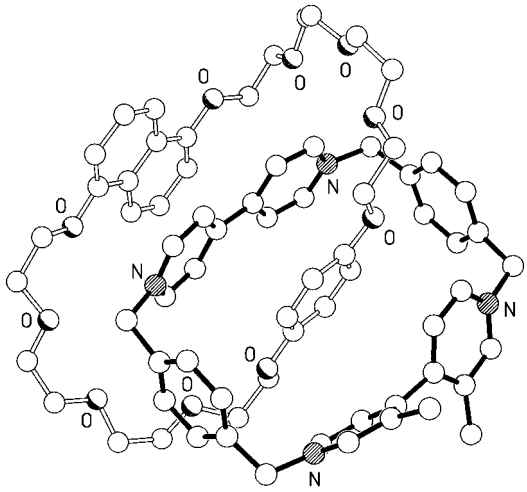

Figure 2. The solid-state structure of the [2]catenane **7**$^{4+}$. The C–H$\cdots\pi$ interactions between the inside hydroquinone ring and the two paraxylyl units have H$\cdots\pi$, C–H$\cdots\pi$, upper, 2.74 Å, 164°; lower, 2.78 Å, 162°. C–H$\cdots$O hydrogen bonds are between the upper α-CH-bipy hydrogen atom and the central oxygen atom of the upper polyether loop and between the lower inside CH_2 group of the tetracationic cyclophane and the second oxygen along the polyether chain from the outside 1,5-dioxynaphthalene ring system. The respective geometries are C$\cdots$O, H$\cdots$O, C–H$\cdots$O, 3.20, 2.28 Å, 159°; 3.27, 2.42 Å, 148°.

The solid-state geometry (Figure 4) of the [2]catenane **8**$^{4+}$ departs from the C_2 symmetric arrangement observed for the other two [2]catenanes in that its outside 1,5-dioxynaphthalene ring system is displaced with respect to the molecular C_2 axis, such that it is positioned preferentially over one of the pyridinium rings of the inside bipyridinium unit. The mean interplanar separation between the outside 1,5-dioxynaphthalene ring system and this inside pyridinium ring is only 3.28 Å, whereas those between the inside 1,5-dioxynaphthalene ring system and the inside bipyridinium and outside bipicolinium ring systems are 3.35 and 3.64 Å, respectively. This last separation is significantly less than that which was observed in the solid-state structures **6**$^{4+}$ and **7**$^{4+}$ and is clearly a consequence of the significantly reduced torsional twist (46°, cf. 60°) associated with the outside bipicolinium unit: the torsional twist of the inside bipyridinium unit is 4°. Stabilization of the [2]catenane co-conformation is achieved by the familiar range of $\pi\cdots\pi$, C–H$\cdots\pi$, and C–H$\cdots$O interactions. There are no additional $\pi\cdots\pi$ stacking interactions that extend beyond the molecule.

The [3]catenane **9**$^{8+}$ has crystallographic inversion symmetry (Figure 5), the macrocyclic octacation adopting an open

  0947-6539/03/0902-0545 $ 20.00+.50/0

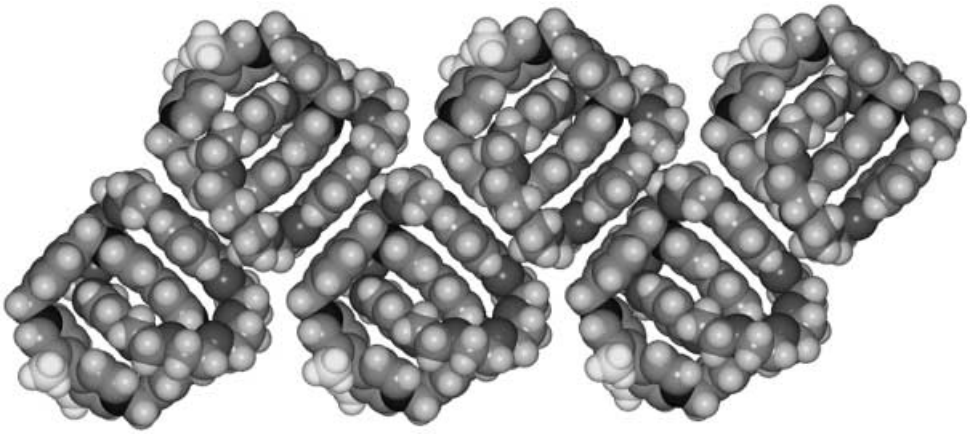

Figure 3. A space-filling representation of part of one of the π–π stacked tapes present in the solid-state superstructure of the [2]catenane $\mathbf{7}^{4+}$.

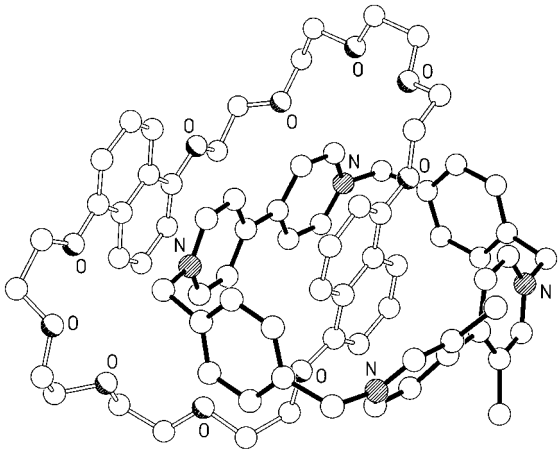

Figure 4. The solid-state structure of the [2]catenane $\mathbf{8}^{4+}$. The C–H···π interactions between the inside 1,5-dioxynaphthalene ring system and the paraxylyl units have H···π, C–H···π, upper, 2.48 Å, 151°; lower 2.54 Å, 151°. There is a bifurcated C–H···O hydrogen bond between the uppermost α-CH-bipy hydrogen atom and the second and third oxygen atoms from the inside 1,5-dioxynaphthalene ring system. Also, there are C–H···O hydrogen bonds a) between the lowermost α-CH-bipy hydrogen atom from the inside 1,5-dioxynaphthalene ring system in the lower polyether loop and b) between the lower inside CH_2 group of the tetracationic cyclophane and the second oxygen atom from the outside 1,5-dioxynaphthalene ring system. The respective geometries are C···O, H···O, C–H···O, 3.15, 2.36 Å, 139°; 3.15, 2.32 Å, 145°; 3.14, 2.31 Å, 145°; 3.13, 2.27 Å, 149°.

extended conformation with a significant free pathway through its center. The voids so formed are filled with MeCN solvent molecules. The transannular separation between the centers of the central linking bonds of the bipicolinium units is 12.6 Å. These units display a substantial twist angle between their constituent pyridinium rings. In contrast to the ordered positioning of the methyl substituents on the bipicolinium units in all three [2]catenanes, in the solid-state structure of this [3]catenane, the positioning of the methyl substituents on one of the bipicolinium units exhibits 0.75:0.25 inside:outside disorder. The inside bipyridinium unit has a substantially greater torsional twist (23°) than in any of the three [2]catenanes. The separation between the inside bipyridinium unit and the inside and outside hydroquinone rings are 3.57 and 3.53 Å, respectively. In this structure, since there are no C–H···π interactions, stabilization is by π···π and C–H···O interactions. There are no inter[3]catenane interactions of note.

In the solid state (Figure 6), the [3]catenane $\mathbf{11}^{8+}$, in which the π-electron-rich components are all 1,5-dioxynaphthalene ring systems, has a dramatically different and substantially more compact structure. The molecule has both crystallographic and molecular C_2 symmetry about an axis passing through the centers of the two linking C–C bonds of the pair of bipicolinium units: their centroids are separated by a mere 4.05 Å. The torsional twist angles in the two independent bipicolinium units are 68° and 59°, whereas that for the unique inside bipyridinium unit is only 7°. The separation between this unit and the inside and outside 1,5-dioxynaphthalene ring systems is 3.44 Å in each case. Again, there are no C–H···π interactions, only π···π and C–H···O ones. The packing of the molecules is complex and comprises a contiguous three

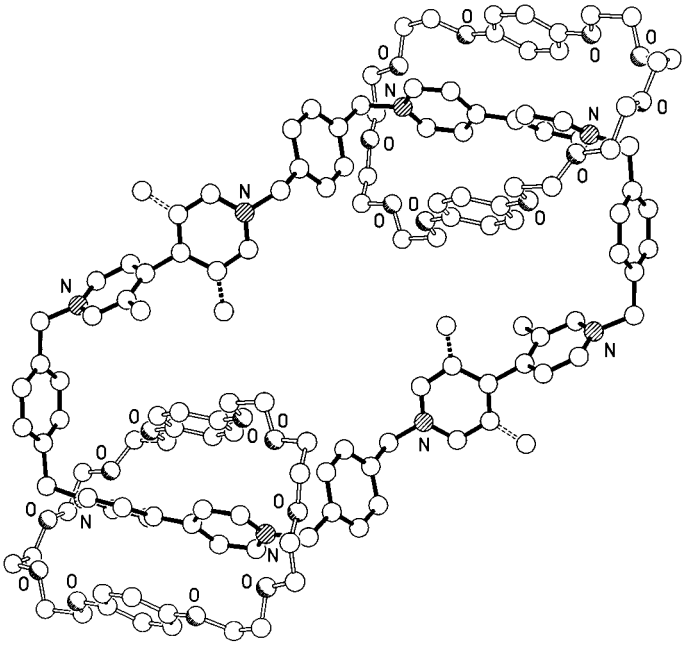

Figure 5. The solid-state structure of the [3]catenane $\mathbf{9}^{8+}$. There are C–H···O hydrogen bonds between the pair of CH_2 groups attached to the inside bipyridinium units and the central oxygen atoms of the proximal polyether loops. Their respective geometries are C···O, H···O, C–H···O, 3.37, 2.44 Å, 162°; 3.35, 2.40 Å, 170°,

0947-6539/03/0902-0546 $ 20.00+.50/0 *Chem. Eur. J.* **2003**, *9*, No. 2

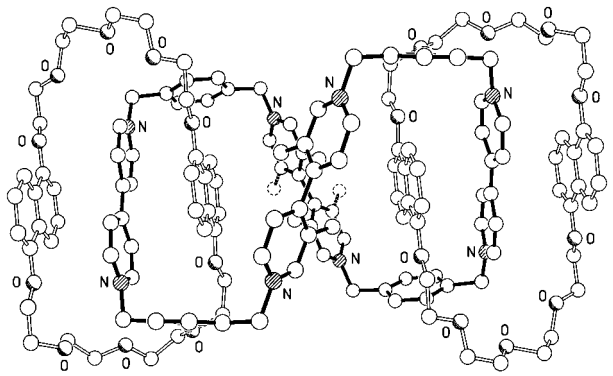

Figure 6. The solid-state structure of the [3]catenane $\mathbf{11}^{8+}$. There are C–H···O hydrogen bonds a) between the upper left CH_2 group associated with the inside bipyridium unit and the central oxygen atom of the proximal polyether loop and b) between the lower α-CH-bipy hydrogen atom and the central oxygen atom of the proximal polyether loop. Their respective geometries are C···O, H···O, C–H···O, 3.21, 2.25 Å, 177°; 3.23, 2.38 Å, 147°.

dimensional net formed by inter[3]catenane $\pi-\pi$ stacking of the outside 1,5-dioxynaphthalene ring systems of one molecule and pairs of paraxylyl units in another. The mean interplanar separation is ca. 3.65 Å.

Dynamic ^{1}H NMR spectroscopy: To achieve a better understanding of the switching properties of the molecules in solid-state catenane-based devices,[10] and to bring about improvements in the design of molecular switches, an in-depth understanding of the dynamic behavior of the molecules in solution must be attained. Toward this end, a detailed dynamic ^{1}H NMR kinetic study[22] has been carried out on all three of the [2]catenanes, namely $\mathbf{6}\cdot 4PF_6$, $\mathbf{7}\cdot 4PF_6$ and $\mathbf{8}\cdot 4PF_6$, with the objective of obtaining a better appreciation of 1) the nature of the noncovalent bonding interactions between the two macrocyclic ring compounds and 2) the rates of the relative movements, including rocking and circumrotations, of the ring components, as well as degenerate rotations of the para-disubstituted aromatic rings. An analogous series of experiments on the [3]catenanes, $\mathbf{9}\cdot 8PF_6$, $\mathbf{10}\cdot 8PF_6$ and $\mathbf{11}\cdot 8PF_6$, was precluded by the fact that the degenerate and relative movements of the parts and components in these molecules are much too fast in solution to be detected on the ^{1}H NMR timescale, even at very low temperatures. The difference between the [2]- and [3]catenanes must reflect the relative compactness of the former and the relative looseness of the latter—a feature which is immediately evident from an inspection of CPK space-filling molecular models. Thus, in this section, the various dynamic processes present in the [2]catenanes are discussed and compared across the series $\mathbf{6}^{4+}$, $\mathbf{7}^{4+}$, and $\mathbf{8}^{4+}$.

In parent tetracationic cyclophanes, aromatic ring rotations typically occur too rapidly to affect ^{1}H NMR line shapes, even at very low temperatures. However, on account of their sterically constricted nature as interlocked components in [2]catenanes, the activation barriers for some of these rotational processes have been observed to increase dramatically. Two such processes were observed in all three [2]catenanes—one involving rotation of the phenylene rings in the tetracationic cyclophanes and the other involving rotation of their pyridinium rings. In the [2]catenanes, whereas the encircled bipyridinium unit is oriented face-to-face with the two aromatic ring systems in the crown ether component, the phenylene rings experience only a single, weak edge-to-face interaction with the encircled aromatic ring of the crown ether component. Rapid rotation (Figure 7a) of the phenylene rings on the ^{1}H NMR timescale results in an exchange process,

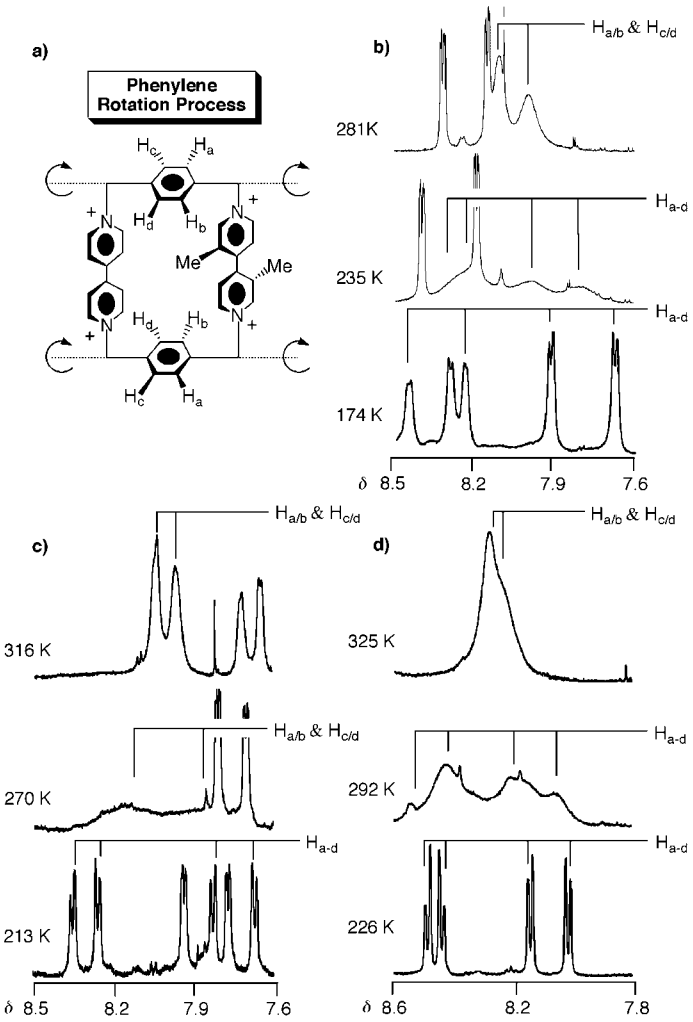

Figure 7. a) A schematic representation of the phenylene ring rotation process occurring simultaneously in both paraxylylene spacers in the tetracationic cyclophane component of the [2]catenanes. Rotation of the phenylene rings around their substituted axis causes exchange between H_a and H_b, and H_c and H_d. Selected ^{1}H NMR spectra recorded in CD_3COCD_3 for b) $\mathbf{6}\cdot 4PF_6$, c) $\mathbf{7}\cdot 4PF_6$, and d) $\mathbf{8}\cdot 4PF_6$, showing the coalescences of the peaks corresponding to the phenylene ring protons on the tetracationic cyclophane component as the temperature is increased.

wherein the four observed signals (Figure 7b–d) for the phenylene rings at low temperatures collapse into two signals when the temperature is raised. The site exchanges occur such that H_a and H_b, as well as H_c and H_d, are interconverted. If we assume, for the time-being at least, that the rocking of the crown ether ring has no observable effect on the magnetic equivalence of these phenylene protons, and the two phenylene rings in the tetracationic cyclophane are equivalent because of C_2 symmetry, then the observation of four signals

at low temperature can be rationalized. The protons H_a and H_c are *anti* to the methyl group on the closest picolinium ring with respect to the plane containing the four nitrogen atoms of the cyclophane, while the protons H_b and H_d are *syn* to this methyl group. Additionally, H_a and H_b are closer to the bipicolinium than to the bipyridinium unit, while H_c and H_d are further away. Thus, all four phenylene protons on each ring are heterotopic. The kinetic and thermodynamic data for phenylene ring rotations are recorded in Table 1 for all three

Table 1. Phenylene rotation kinetic and thermodynamic data in CD_3COCD_3.

[2]Catenane	T [K][a]	k_{ex} [s^{-1}][b]	$\Delta G^{\ddagger}$ [kcal mol^{-1}][c]
6·4PF_6[d]	174	0.17	10.6
	182	0.35	10.9
7·4PF_6[e]	191	0.08	12.0
	202	0.26	12.2
	213	1.0	12.3
	225	2.6	12.6
8·4PF_6[f]	217	0.17	13.3
	227	0.63	13.4
	238	1.53	13.6
	249	3.89	13.8
	259	10.9	13.9

[a] Calibrated by using a neat MeOH sample. [b] Measured by using spin saturation transfer method. See ref. [22]. [c] ± 0.1 kcal mol^{-1}. [d] Exchange observed between peaks corresponding to the protons on the phenylene ring of the tetracationic cyclophane at $\delta = 7.92/8.45$ and 7.68/8.25 ppm. [e] Exchange observed between peaks corresponding to the protons on the phenylene ring of the tetracationic cyclophane at $\delta = 7.84/8.35$ and 7.67/8.26 ppm. [f] Exchange observed between peaks corresponding to the protons on the phenylene ring of the tetracationic cyclophane at $\delta = 8.14/8.48$ and 8.02/8.44 ppm.

[2]catenanes. Although direct quantitative comparisons of the $\Delta G^{\ddagger}$ values are precluded by the lack of kinetic data for all three compounds at the same temperature, qualitatively it is clear that the barrier for phenylene ring rotation increases through the series $\mathbf{6}^{4+}$ to $\mathbf{7}^{4+}$ to $\mathbf{8}^{4+}$ by about 1 kcal mol^{-1} from one to the other. This trend correlates with the increasing number of 1,5-dioxynaphthalene recognition sites in the crown ether ring component of the [2]catenanes. This phenomenon cannot be rationalized solely by steric interactions with the inside aromatic unit of the crown ether component, because, if this were the case, one would only expect a significant affect by changing the inside aromatic unit of the crown ether component. On the contrary, changing only the outside aromatic unit from hydroquinone to 1,5-dioxynaphthalene increases the barrier for phenylene rotation.

A possible explanation for this barrier increase involves steric interactions with the glycol chains. On account of the orientation of the outside 1,5-dioxynaphthalene ring system, the glycol chain comes into closer contact with the phenylene ring of $\mathbf{7}^{4+}$ than it does when there is an outside hydroquinone ring present in the crown ether macrocycle. This difference can be easily appreciated on comparing the corresponding X-ray crystal structures and examining the close contact distances between the crown ether macrocycle and the tetracationic cyclophane. These closer and hence stronger interactions render it less easy for the phenylene rings in the tetracationic cyclophane component to rotate.[23]

The independent rotations of both pyridinium rings within the bipyridinium units in the tetracationic cyclophane component of the [2]catenanes interchanges pairs of nonequivalent protons in these units (Figure 8a). In common with the

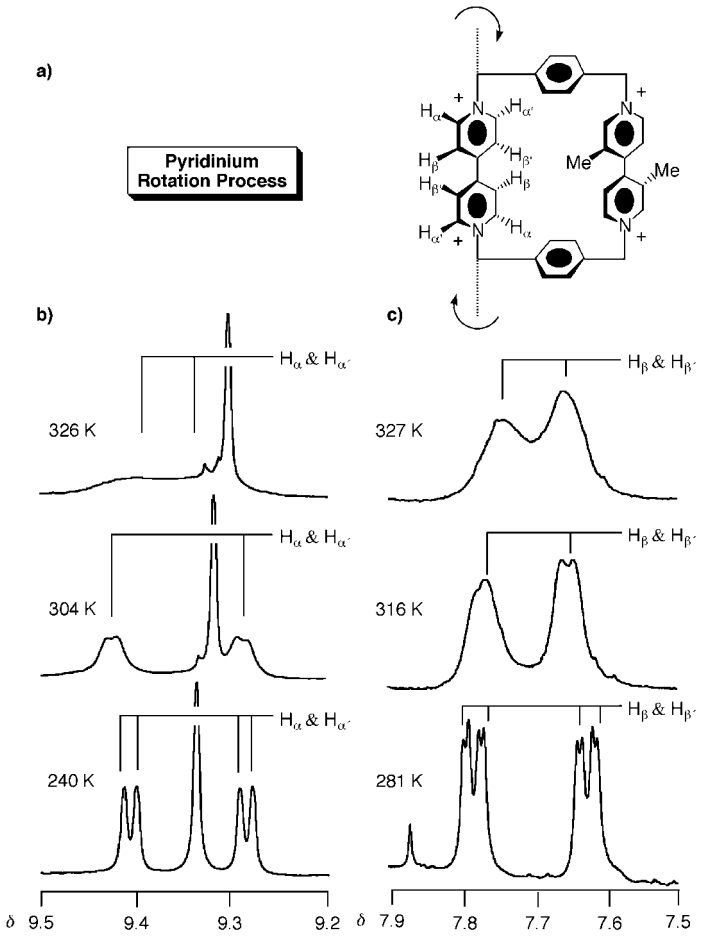

Figure 8. a) A schematic representation of the pyridinium ring rotation process occurring simultaneously in both halves of the bipyridinium unit present in the tetracationic cyclophane component of the [2]catenanes. Rotation of the pyridinium rings independently around the axis of the bipyridinium unit brings about the exchange of H_α with $H_{\alpha'}$ and H_β with $H_{\beta'}$. Selected ^1H NMR spectra recorded in CD_3COCD_3 for b) **6**·4PF_6 and c) **7**·4PF_6 showing the coalescences of peaks corresponding to the pyridinium ring protons on the tetracationic cyclophane component as the temperature is increased.

phenylene ring rotations, the slow exchange limit for pyridinium ring rotations reveals four signals, which coalesce into two signals at higher temperatures (Figure 8b and c). The nonequivalence of the pyridinium protons is a consequence of their different topic relationships with respect to the methyl groups in the bipicolinium unit, as well as of their different constitutions. While H_α and H_β are *syn* to the methyl group in the closer picolinium ring, $H_{\alpha'}$ and $H_{\beta'}$ are *anti*. Both pyridinium rings in the bipyridinium unit are equivalent by C_2 symmetry. Rotation of either pyridinium ring results in site exchange between H_α and $H_{\alpha'}$ and between H_β and $H_{\beta'}$. The kinetic and thermodynamic data for this process are listed in Table 2. Comparison of the activation barriers at 293 K shows that changing the outside aromatic residue in the crown ether

0947-6539/03/0902-0548 $ 20.00+.50/0 *Chem. Eur. J.* **2003**, *9*, No. 2

Table 2. Pyridinium rotation kinetic and thermodynamic data in CD_3COCD_3.

[2]Catenane	T [K][a]	k_{ex} [s^{-1}]	$\Delta G^{\ddagger}$ [kcal mol^{-1}][d]
6·4PF_6[e]	247	0.20[b]	15.2
	256	0.48[b]	15.3
	270	1.3[b]	15.6
	281	3.5[b]	15.7
	293	7.7[c]	15.9
	304	18[c]	16.1
	316	42[c]	16.2
7·4PF_6[f]	270	0.08[b]	17.1
	281	0.36[b]	17.0
	293	1.4[b]	17.0
	305	4.3[b]	17.0
8·4PF_6[g]	292	1.15[b]	17.0
	305	3.35[b]	17.1

[a] Calibrated by using a neat MeOH sample. [b] Measured by using spin saturation transfer method. See ref. [22]. [c] Measured by using line shape analysis method. [d] ±0.1 kcal mol^{-1}. [e] Exchange observed between the H_α and $H_{\alpha'}$ peaks of the pyridinium rings in the tetracationic cyclophane at 9.41 and 9.29 ppm. [f] Exchange observed between the H_β and $H_{\beta'}$ peaks of the pyridinium rings in the tetracationic cyclophane at 7.67 and 7.58 ppm. [g] Exchange observed between the H_β and $H_{\beta'}$ peaks of the pyridinium rings in the tetracationic cyclophane at 7.24 and 7.06 ppm.

component from a hydroquinone ring to a 1,5-dioxynaphthalene ring system results in an increase of approximately 1 kcal mol^{-1} in the rotational barrier. However, changing the second aromatic residue to a 1,5-dioxynaphthalene ring system has no further effect on the barrier to pyridinium ring rotation. It seems that the 1/5NPP36C10 macrocycle is as good a match for the tetracationic cyclophane as is the 1/5DNP38C10 one, a feature which is apparent in the yields (11 and 9%, respectively) obtained during the template-directed synthesis of **7**·4PF_6 and **8**·4PF_6 (see Scheme 1). The process of pyridinium ring rotation in these three [2]catenanes is undoubtedly intimately tied up with other mechanical processes going on simultaneously in these molecules.

A third possible rotational process in the tetracationic cyclophane components of $\mathbf{6}^{4+}$, $\mathbf{7}^{4+}$, and $\mathbf{8}^{4+}$ is that involving the independent rotations of the two picolinium rings in the bipicolinium unit. This process, which is not observable by dynamic ^{1}H NMR spectroscopy in an accessible temperature range, would be expected to have a very large barrier in these three [2]catenanes. In order to rotate one picolinium ring with respect to the other, the two methyl groups would either have to pass by each other or one of them would have to pass through the cavity of the tetracationic cyclophane. Inspection of CPK space-filling molecular models suggests that the latter process is nigh impossible. Also, literature data on analogously substituted bipicolines reveal very high barriers to rotations in these molecules.[24] Although this process may be observable at very high temperatures by ^{1}H NMR spectroscopy, it is not going to proceed at a rate at lower temperatures that will influence other ring rotation processes.

A mechanical process, however, which should be observable in the two degenerate [2]catenanes $\mathbf{6}^{4+}$ and $\mathbf{8}^{4+}$ is that of circumrotation of the crown ether ring with respect to the tetracationic cyclophane component.[25] Circumrotation of the crown ether macrocycle through the cavity of the tetracationic cyclophane results (Figure 9) in the equilibration of the two

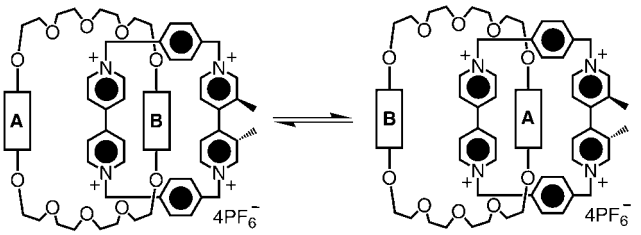

Figure 9. A schematic representation of the crown ether circumrotational process in the [2]catenanes. The equilibration between the two forms is degenerate in the case of $\mathbf{6}^{4+}$ and $\mathbf{8}^{4+}$ and nondegenerate for $\mathbf{7}^{4+}$, that is, it can undergo translational isomerism.

identical aromatic rings between the inside and outside positions in $\mathbf{6}^{4+}$ and $\mathbf{8}^{4+}$. In the case of the nondegenerate [2]catenane $\mathbf{7}^{4+}$, the overwhelming preference for its having the hydroquinone ring located inside the cavity of the tetracationic cyclophane with the 1,5-dioxynaphthalene ring system residing outside (as observed in the solid-state structure illustrated in Figure 2) means that dynamic ^{1}H NMR spectroscopy cannot be employed to probe a circumrotational process which is undoubtedly operative. The reason is that the other (very minor) translational isomer cannot be identified in the low temperature spectrum.

The kinetic and thermodynamic data (Table 3) for the crown ether ring circumrotation in $\mathbf{6}^{4+}$ and $\mathbf{8}^{4+}$ show a larger barrier for the second of these two [2]catenanes by around 1.2 kcal mol^{-1}. This difference presumably arises from the stronger interaction of the 1/5DNP38C10 ring with the tetracationic cyclophane than it experiences with BPP34C10. It is evident from a comparison of the two X-ray crystal structures, illustrated in Figures 4 and 1, respectively, that C–H···O and C–H···π interactions, as well as π···π stacking interactions, are much more significant in the former than in the latter. Another interesting feature evident from a perusal of the data in Table 3 is the trend in $\Delta G^{\ddagger}$ values from larger to smaller with increasing temperature, indicative of a positive $\Delta S^{\ddagger}$ value. An Eyring plot, which is shown in Figure 10, gives a $\Delta S^{\ddagger}$ value of 7.4 cal mol^{-1} K^{-1} for **6**·4PF_6. This positive

Table 3. Crown ether ring circumrotation kinetic and thermodynamic data in CD_3COCD_3.

[2]Catenane	T [K][a]	k_{ex} [s^{-1}]	$\Delta G^{\ddagger}$ [kcal mol^{-1}][d]
6·4PF_6[e]	256	0.2 [c]	15.7
	270	1.2[c]	15.6
	281	5.6[c]	15.5
	293	21[c]	15.4
	304	60[c]	15.4
	316	180[c]	15.3
	326	450[c]	15.2
7·4PF_6		not observed	
8·4PF_6[f]	271	0.13[b]	16.9
	282	0.57[b]	16.8
	293	2.56[b]	16.6

[a] Calibrated by using a neat MeOH sample. [b] Measured by using spin saturation transfer method (ref. [22]). [c] Measured by using line shape analysis method. [d] ±0.1 kcal mol^{-1}. [e] Exchange observed between the peaks corresponding to the outside (6.27 ppm) and inside (3.84 ppm) hydroquinone rings of the crown ether component. [f] Exchange observed between peaks corresponding to the outside (7.28 ppm) and inside (2.70 ppm) 1,5-dioxynaphthalene rings of the crown ether component.

  0947-6539/03/0902-0549 $ 20.00+.50/0

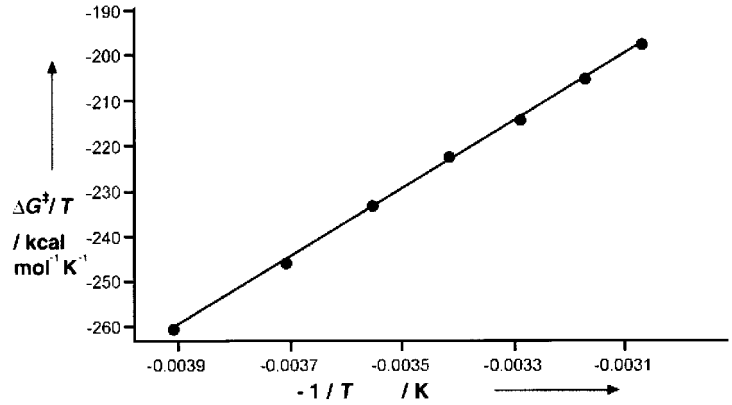

Figure 10. The Eyring plot for crown ether circumrotation in $\mathbf{6}^{4+}$. Using a linear least-squares fit, the following equation was obtained: $(-\Delta G^{\ddagger}/T) = (17.6\ \text{kcal mol}^{-1})(-1/T) + (7.4\ \text{cal mol}^{-1}\text{K}^{-1})$.

entropy of activation indicates that the transition state for circumrotation of the BPP34C10 ring around the tetracationic cyclophane is entropically more favored, that is, more flexible, than the ground state co-conformation and/or that the transition state is less well solvated than the ground state, causing a release of molecules of solvation into the bulk solvent during the circumrotational process. Since, at the transition state, most, if not all, of the noncovalent bonding interactions between the two interlocked components will have been ripped apart, a more flexible co-conformation should result. Also, a highly solvated ethyleneglycol chain has to pass through the middle of the tetracationic cyclophane during the circumrotational process and in so doing has presumably to cast off some molecules of solvation, which will not be attracted to the bare hydroquinone rings freed of their $\pi\cdots\pi$ stacking interactions.

The tilting of the crown ether rings with respect to the mean plane of the tetracationic cyclophane has already been discussed for the two [2]catenanes $\mathbf{6}^{4+}$ and $\mathbf{7}^{4+}$, in which a hydroquinone ring resides inside the cavity of the cyclophane. This tilt gives rise to a rocking process,[26] wherein one co-conformation is in rapid equilibrium on the ^{1}H NMR timescale with another co-conformation. In the absence of any other chiral element in the [2]catenane molecule, the equilibration process is tantamount to the inversion of enantiomers as shown in Figure 11a, whereby the source of chirality is helical.[26, 27] However, if another element of chirality is present in the molecule, then it becomes possible to analyze the rocking in the [2]catenane in terms of the interconversion between diastereoisomeric pairs of enantiomers. All three [2]catenanes possess an axis of chirality[27] on account of the atropisomerism exhibited by the bipicolinium unit (Figure 11b). The combination of helical and axial chirality in $\mathbf{6}^{4+}$ gives rise to the possibility of the existence of two diastereoisomers in the form of enantiomeric pairs (Figure 12). The situation is further complicated in $\mathbf{7}^{4+}$ and $\mathbf{8}^{4+}$ by the presence of one and two 1,5-dioxynaphthalene rings (Figure 11c), which add on additional elements of planar chirality,[26, 28] increasing the number of enantiomeric pairs of diastereoisomers to four (Figure 13) and eight (Figure 14), respectively. Although in the case of all three [2]catenanes, only one diastereoisomer is identified in the solid state by X-ray crystallography (see Figures 1, 3, and 4 for $\mathbf{6}^{4+}$, $\mathbf{7}^{4+}$, and $\mathbf{8}^{4+}$, respectively), it is even more important to note that in solution, at least at those temperatures at which all the significant dynamic processes become slow on the ^{1}H NMR timescale, only *one* diastereoisomer—most likely the same one as in the solid state—prevails for the most part. We shall return to a discussion of this topic later. Suffice to say at this juncture that, in the case of the [2]catenane $\mathbf{8}^{4+}$ in particular, there is a dynamic combinatorial library[29] of possible structures (Figure 14), wherein the free energies of the various stereoisomers decide which is going to be by far the most dominant one.[30]

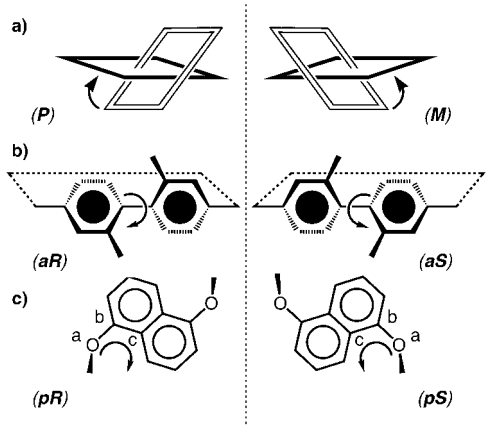

Figure 11. Our definition of the absolute stereochemical descriptors. The helicities of plus and minus are indicated by (*P*) and (*M*), respectively. We give the open, unshaded ring (containing oxygen atoms) a higher priority than the full, shaded ring and, on that basis, display the open ring in front of the shaded ring when defining the helicities generated by the two rings. The axial chiralities of the bipicolinium units are denoted by the symbols (*aR*) and (*aS*) and the planar chiralities of the 1,5-dioxynaphthalene ring systems by the symbols, (*pR*) and (*pS*). The rules used to describe these two forms of chirality are essentially those discussed in ref. [27d].

The ring-rocking process can be probed by means of the ^{1}H NMR signals for the inside hydroquinone ring in the macrocyclic polyether components in the [2]catenanes $\mathbf{6}^{4+}$ and $\mathbf{7}^{4+}$ (Table 4). One pair of hydroquinone ring protons—those involved in C–H$\cdots\pi$ interactions with the paraxylylene rings in the tetracationic cyclophane—is highly shielded as a result of the stable co-conformation shown in Figure 15. The result is an upfield shift, by about 4 ppm, of the signal for these protons. Exchange between these shielded protons and the pair of ′exposed′ protons occurs during the ring-rocking process and provides a means to observe this motion. One would expect a low barrier for this process because only the weak C–H$\cdots$O and C–H$\cdots\pi$ interactions have to be broken, while $\pi\cdots\pi$ stacking interactions are perturbed, but presumably not lost altogether. Thus, the ring-rocking process should

0947-6539/03/0902-0550 $ 20.00+.50/0 *Chem. Eur. J.* **2003**, *9*, No. 2

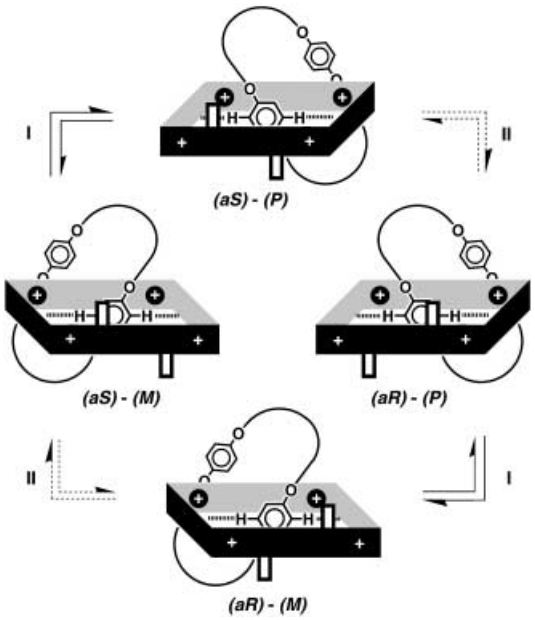

Figure 12. The processes (I and II) for interconverting diastereoisomers and inverting enantiomers in the [2]catenane $\mathbf{6}^{4+}$. Process I corresponds to inversion of the helical chirality while process II represents an inversion of the axial chirality. The descriptors of absolute stereochemistry are defined in Figure 11. Note that process I occurs easily, whereas process II would only occur with difficulty. Not all the possible interconversion pathways for processes I and II are shown.

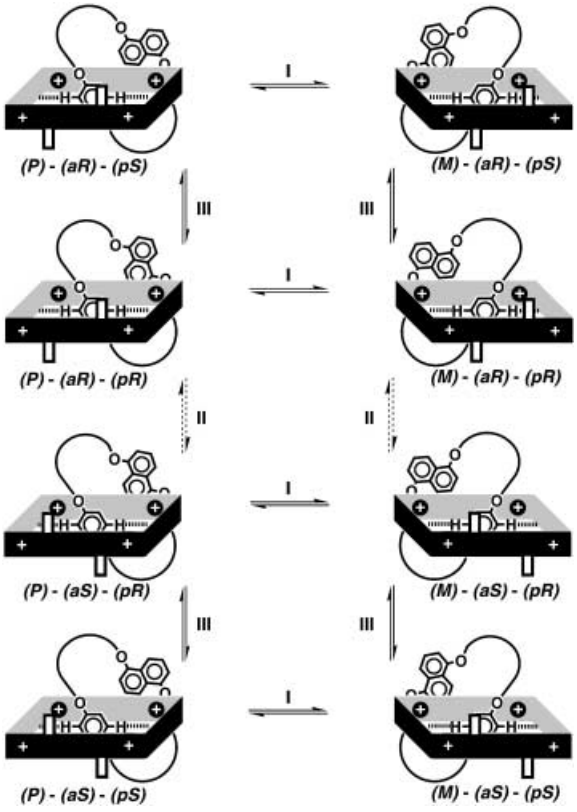

Figure 13. The processes (I, II, and III) for interconverting diastereoisomers and enantiomers in the [2]catenane $\mathbf{7}^{4+}$. Process I corresponds to inversion of the helical chirality, process II, which would only occur with difficulty, corresponds to inversion of the axial chirality, and process III corresponds to inversion of the planar chirality. The descriptors of absolute stereochemistry are defined in Figure 11. Not all the possible interconversion pathways for processes I, II, and III are shown.

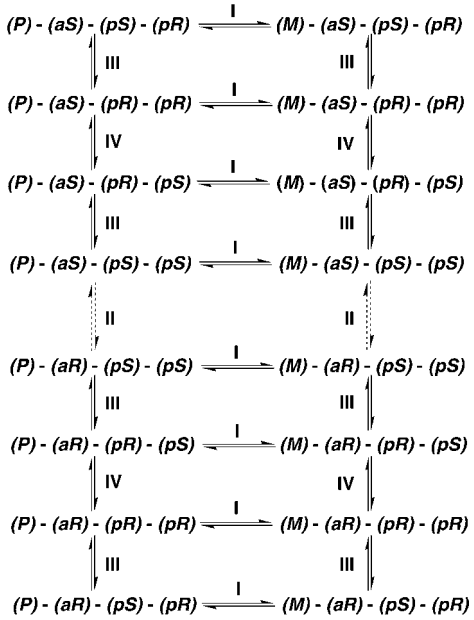

Figure 14. The processes I–IV associated with the interconversion of diastereoisomers and with the inversion of enantiomers in the [2]catenane $\mathbf{8}^{4+}$. Process I corresponds to inversion of the helical chirality, process II, which would only occur with difficulty, corresponds to inversion of the axial chirality, and processes III and IV correspond to inversions of the planar chiralities. The descriptors of absolute stereochemistry are defined in Figure 11. Not all possible interconversions are shown. Not all the possible interconversion pathways for processes I, II, III, and IV are shown.

Table 4. Ring rocking kinetic and thermodynamic data in CD_3COCD_3.

[2]Catenane	T [K][a]	k_{ex} [s^{-1}][b]	$\Delta G^{\neq}$ [kcal mol^{-1}][c]
$\mathbf{6}\cdot 4PF_6$[d]	174	1.22	9.9
	182	2.53	10.2
$\mathbf{7}\cdot 4PF_6$[e]	234	1.81	13.3
$\mathbf{8}\cdot 4PF_6$	not observed		

[a] Calibrated by using a neat MeOH sample. [b] Measured by using spin saturation transfer method (ref. [22]). [c] ± 0.1 kcal mol^{-1}. [d] Exchange observed between the peaks corresponding to the protons of the inside hydroquinone ring of the crown ether component at 5.43 and 2.25 ppm. [e] Exchange observed between the peaks corresponding to the protons of the inside hydroquinone ring of the crown ether component at 5.26 and 2.18 ppm.

occur extremely rapidly and would normally be very difficult to observe if it were not for the fortuitous fact that the large chemical shift difference,[31] which results from the shielding effect (Figure 15), allows for the observation of this fast process at the lower limit of the temperature range for CD_3COCD_3. As a result of the stereochemical issues discussed earlier and illustrated in Figures 12 and 13, the site exchange process is not simple and straightforward, since it involves equilibration between two diastereoisomers—a minor one and a major one. This situation was confirmed by careful double irradiation experiments carried out at 182 K on resonances for the [2]catenane $\mathbf{6}\cdot 4PF_6$. Irradiation of the lower intensity peak centered on $\delta = 5.4$ ppm, which corresponds to the minor diastereoisomer (Figure 16), resulted in a decrease in the intensity of the higher intensity peak centered on $\delta = 2.3$ ppm, which corresponds to the major diastereoisomer. To confirm that this observation is the result of a

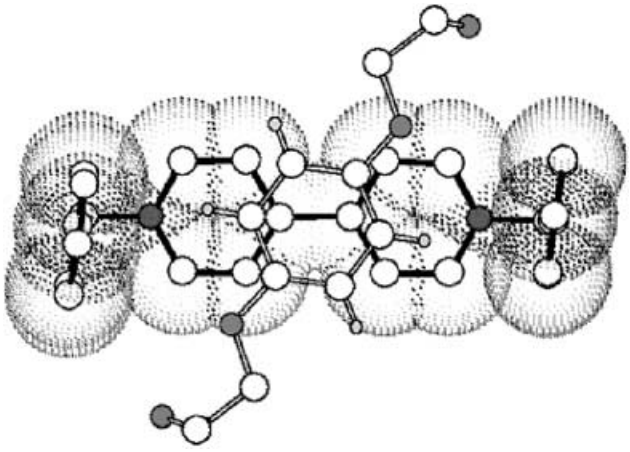

Figure 15. This cut-away illustration reveals the origin of the very large limiting chemical shift difference for the inside hydroquinone protons when the rocking process, involving the crown ether ring and the tetracationic cyclophane, becomes slow on the ^{1}H NMR timescale. Two distinct pairs of hydroquinone protons can be identified, those that are involved in C–H$\cdots\pi$ interactions with the bridging paraxylylene units in the tetracationic cyclophane and are therefore highly shielded and those that are exposed to the solvent and are not shielded.

saturation transfer effect, and not a simple NOE, the irradiation was also performed at an equal distance on the opposite side of the large peak at $\delta = 5.5$ ppm. The resulting decrease in intensity of the peak at $\delta = 2.3$ ppm was much smaller, confirming that the observed spectra are a result of a site-exchange process. If we were observing an NOE from the off-resonance irradiation of the large peak, then the intensity would decrease equally in both cases. For the [2]catenane **6**·4PF$_6$, the ratio between the two diastereoisomers was determined to be 100:5 by integration of the ^{1}H NMR spectrum (Figure 16) recorded at 182 K in CD_3COCD_3. This ratio corresponds to a ΔG° value of 1.1 kcal mol^{-1} in favor of the major diastereoisomer.[32] To confirm that this isomer is the same as the one [(*aS*)-(*M*)/(*aR*)-(*P*) in Figure 12] present in the solid-state (Figure 1), molecular mechanics calculations were performed[33] on **6**$^{4+}$. The details of these calculations will be discussed in a future publication. However, preliminary results indicate a ΔE value of 1.6 kcal mol^{-1} in favor of the (*aS*)-(*M*)/(*aR*)-(*P*) diastereoisomer. It should be noted that the $\Delta G^{\ddagger}$ values reported in Table 4 for ring rocking are for the minor-to-major diastereoisomer. The ^{1}H NMR chemical shifts for the inside and outside aromatic ring systems in the major diastereoisomers of **6**$^{4+}$, **7**$^{4+}$, and **8**$^{4+}$ are summarized in Table 5. In the case of the [2]catenane **7**·4PF$_6$, we can only surmise that the major diastereoisomer populated in solutions is the (*M*)-(*aS*)-(*pR*)/(*P*)-(*aR*)-(*pS*) one (Figure 13) observed in the solid-state structure (Figure 2). It is intriguing that the ring-rocking process for **7**$^{4+}$ has a free energy barrier at least 3 kcal mol^{-1} higher than that obtained for **6**$^{4+}$ (Table 4). This difference can probably be attributed to the need for the outside 1,5-dioxynaphthalene ring system to undergo inversion of its local chirality, at considerable cost to its $\pi\cdots\pi$ stacking interactions, when ring rocking occurs. Finally, when we reach the [2]catenane **8**·4PF$_6$ with an inside, as well as an outside 1,5-dioxynaphthalene ring system, ring rocking is no longer an option: it cannot occur. Also, diastereoselection is probably complete for this [2]catenane in solution for the (*M*)-(*aS*)-(*pR*)-(*pR*)/(*P*)-(*aR*)-(*pS*)-(*pS*) racemic mixture, which is the form that crystallizes out in the solid-state (Figure 4). The ^{1}H NMR chemical shifts listed in Table 5 for the outside 1,5-dioxynaphthalene ring system protons in **7**·4PF$_6$ and **8**·4PF$_6$ are not too dissimilar under very similar conditions. It is, therefore, not unreasonable to conclude that the relative planar chiralities of their outside 1,5-dioxynaphthalene ring systems are the same.

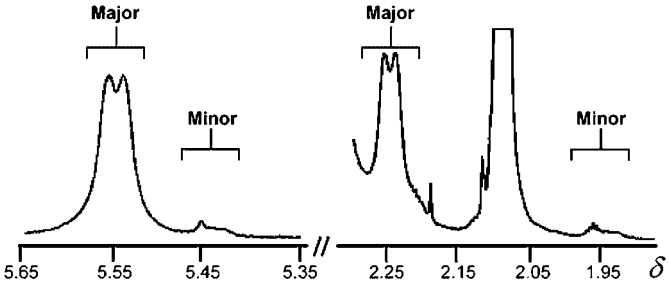

Figure 16. Partial ^{1}H NMR spectrum of **6**·4PF$_6$ recorded in CD_3COCD_3 at 182 K showing the signals for the inside hydroquinone ring protons, as shown in Figure 15, in the major and minor diastereoisomers.

Table 5. ^{1}H NMR chemical shifts (δ values) for the aromatic ring systems of the crown ether macrocycle.[a]

[2]Catenane	T [K][b]	Inner aromatic	Outer aromatic
6·4PF$_6$	182.1	2.26, 5.54	6.23 (br)
7·4PF$_6$	182.7	2.12, 5.38	6.42,[c] 7.18,[d] 7.35[e]
8·4PF$_6$	183.8	2.56,[c] 6.13,[d] 6.26[e]	6.38,[c] 7.05,[d] 7.18[e]

[a] Solvent used was CD_3COCD_3 and the chemical shifts are given in ppm. [b] Calibrated by using a neat MeOH sample. [c] $H_{4/8}$. [d] $H_{3/7}$. [e] $H_{2/6}$.

The ^{1}H NMR spectra recorded in CD_3CN solutions for the three [3]catenanes **9**·8PF$_6$, **10**·8PF$_6$, and **11**·8PF$_6$ indicate as expected that the two macrocyclic polyether rings reside on the two bipyridinium units rather than on the bipicolinium units. We can assume that all three catenanes are composed of rapidly equilibrating diastereoisomeric mixtures, on account of the two different axial chiralities associated with the two bipicolinium units in the octacationic macrocycles—a stereochemical feature that is evident in the solid-state structures of **9**$^{8+}$ and **11**$^{8+}$ shown in Figures 5 and 6, respectively. On account of the fact that the three [3]catenanes all exist as mixtures of inseparable diastereoisomers, it was considered to be unwise to attempt to investigate them further by variable temperature ^{1}H NMR spectroscopy at this juncture.

Conclusion

The fact that donor–acceptor catenanes, incorporating bipicolinium units in their tetracationic cyclophane components and 1,5-dioxynaphthalene components in their crown ether components, have the potential to exhibit both axial and planar chiralities within the same molecules affords them intriguing stereochemical properties. In the case of those [2]catenanes where one macrocyclic ring can undergo rocking with respect to the other, helicity comes into the reckoning as

0947-6539/03/0902-0552 $ 20.00+.50/0 *Chem. Eur. J.* **2003**, *9*, No. 2

yet another source of chirality. The outcome for the three [2]catenanes $\mathbf{6}^{4+}$, $\mathbf{7}^{4+}$, and $\mathbf{8}^{4+}$ is the possible existence of two, four, and eight enantiomeric pairs of diastereoisomers, that is, the stereochemical situation could become extremely complicated for these three interlocked molecular compounds. On the contrary, it is very simple with both $\mathbf{6}^{4+}$ and $\mathbf{7}^{4+}$ existing in solution as one major diastereoisomer and $\mathbf{8}^{4+}$ as exclusively one, at least in so far as we can detect. At first reckoning, it seems to be somewhat remarkable that this relative simplicity can emerge out of so much apparent complexity. If the stereochemical options for the donor–acceptor catenanes discussed herein are likened to an emergent dynamic combinatorial library, then it is clear that the selective molecular recognition processes that operate during the self-assembly, which leads on to their template-directed syntheses under kinetic control, preordain the stereochemical latitude given to these interlocked molecules in the final event. Kinetic control at some stage in a supramolecularly assisted covalent synthesis can express itself subsequently in a thermodynamically controlled stereochemical event for which the dice are really loaded in favor of one outcome. When chirality is expressed in multiple ways in a molecule at a dynamic level, then it would appear that the propensity for diastereoselection can be extremely high. The recent observation[28] that some related [2]catenanes which contain both helical and planar chiralities readily undergo spontaneous resolution on crystallization to give optically active crystals raises some intriguing questions. It seems that a phase change can superimpose enantioselection upon the diastereoselection that has already been predetermined by the molecular recognition and self-assembly processes in the early stages of a template-directed synthesis. The realizaton that there exists highly orchestrated chemical reaction pathways between molecular recognition and self-assembly processes, employing templates to uncover asymmetry and chirality in an efficient manner, could be not unimportant when it comes to the future design and construction of unidirectional molecular switches and machines.

Experimental Section

General methods: All reactions were carried out under an argon atmosphere. Chemicals were purchased from Aldrich and used as received. Solvents were dried according to literature procedures.[34] The bis(hexafluorophosphate) **1**,[10] bipicoline (**2**)[35] and crown ethers, BPP34C10 (**3**),[36] 1,5-NPPP36C10 (**4**),[21] and 1,5-DNP38C10 (**5**)[20] were prepared as described previously in the literature. Thin-layer chromatography (TLC) was carried out on aluminum sheets coated with silica-gel 60F (Merck 5554). The plates were inspected by UV light and, if required, developed in I_2 vapor. Column chromatography was carried out by using silica-gel 60 (Merck 9385, 230–400 mesh). Melting points were determined on an Electrothermal 9100 melting point apparatus and are uncorrected. All ^{1}H and ^{13}C NMR spectra were recorded on either a Bruker ARX500 (500 MHz and 125 MHz, respectively) or Bruker Avance 500 (500 MHz and 125 MHz, respectively). All chemical shifts are quoted in ppm, referenced to TMS. Samples were prepared using CD_3COCD_3 or CD_3CN purchased from Cambridge Isotope Labs and the samples for the kinetic study were degassed by using the freeze-pump-thaw method and sealed under vacuum. Temperatures were calibrated by using a neat MeOH sample[37] before or after each experiment and assumed to remain constant during the experiment. Two methods were used to obtain the kinetic data by NMR spectroscopy. The primary method involved spin saturation transfer (SST) experiments.[22] This was accomplished by irradiation of one of the two exchanging protons. Spectra were then obtained with and without irradiation and the T_{1app} was measured in the presence of irradiation. Details of this method can be found in the references. The second method used involved line shape analysis (LSA). The chemical shifts, line widths, and coupling constants were determined at low temperature and input into the Spinworks[38] NMR spectral simulation program. Simulation of the exchange process and comparison with the experimental spectra allowed for determination of the rate constants. Fast atom bombardment (FAB) mass spectra were obtained by using a ZAB-SE mass spectrometer, equipped with a krypton primary atom beam, and a *m*-nitrobenzyl alcohol matrix was utilized. Cesium iodide or poly(ethylene glycol) were employed as reference compounds. Electron spray mass spectra (ESMS) were measure on a VG ProSpec triple focusing mass spectrometer with MeCN as mobile phase. Microanalyses were performed by Quantitative Technologies, Inc.

General procedure for the preparation of the catenanes: A solution of **1**·$2PF_6$ (203 mg, 0.25mmol), bipicoline (**2**) (45 mg, 0.25 mmol) and crown ether **3**, **4**, or **5** (0.52 mmol), in anhydrous DMF (5 mL) was stirred for 15 d at room temperature. The solvent was removed under reduced pressure and the solid residue was purified by column chromatography [SiO_2: 2M $NH_4Cl_{(aq)}$/MeOH/$MeNO_2$ (7:2:1)] to yield two different colored products which were dissolved in H_2O. In both instances, the addition of NH_4PF_6 afforded a orange/purple precipitate, which was filtered off and washed with H_2O to give, in order of elution, a [3]catenane and a [2]catenane.

[2]Catenane 6·4PF$_6$: Yield: 4%; m.p. 130–132 °C (decomp); ^{1}H NMR (500 MHz, CD_3CN, 25 °C): $\delta = 2.21$ (s, 6H), 3.23–4.10 (m, 36H), 5.59 (d, $J = 13.8$ Hz, 2H), 5.67 (d, $J = 13,8$ Hz, 2H), 5.70(d, $J = 16.6$ Hz, 2H), 5.73(d, $J = 16.6$ Hz, 2H), 6.23 (s, 4H), 6.42 (d, $J = 6.4$ Hz, 2H), 7.60 (s, 2H), 7.65 (s, 2H), 7.71 (d, $J = 7.7$ Hz, 4H), 7.88 (d, $J = 7.7$ Hz, 4H), 8.79 (s, 2H), 8.86 (s, 2H), 9.13 ppm (s, 2H); ^{13}C NMR (125 MHz, CD_3CN, 25 °C): $\delta = 17.6$, 65.1, 65.5, 70.6, 70.5, 125.7, 125.8, 125.8, 125.9, 125.9, 129.6, 132.2, 136.8, 137.4, 138.4, 141.0, 145.8, 146.9, 150.3 ppm; MS (FAB): *m*/*z* (%): 1518 (6) $[M - PF_6]^+$, 1374 (15) $[M - 2PF_6]^+$, 1229 (10) $[M - 3PF_6]^+$; elemental analysis calcd (%) for $C_{66}H_{76}F_{24}N_4O_{10}P_4$ (1665.19): C 47.60, H 4.60, N 3.36; found: C 47.55, H 4.64, N 3.31.

[2]Catenane 7·4PF$_6$: Yield: 11%; m.p. 296–298 °C; ^{1}H NMR (500 MHz, CD_3CN, 25 °C): $\delta = 2.17$ (s, 6H), 3.42 (t, $J = 9.0$, 2H), 3.59–3.72 (m, 8H), 3.78–3.91 (m, 20H), 3.96–4.10 (m, 16H), 5.55 (d, $J = 13.6$, 2H), 5.63 (d, $J = 13.6$ Hz, 2H), 5.67 (d, $J = 13.2$ Hz, 2H), 5.80 (d, $J = 13.2$ Hz, 2H), 6.35 (d, $J = 5.7$ Hz, 2H), 6.38 (d, $J = 7.5$ Hz, 2H), 7.13 (s, 4H), 7.22 (dd, $J = 7.5$, 8.0 Hz, 2H), 7.33 (d, $J = 8.0$ Hz, 2H), 7.66 (s, 4H), 7.82 (s, 4H), 8.07 (d, $J = 7.5$ Hz, 2H), 8.63 (s, 2H), 8.77 (s, 2H), 9.01 ppm (s, 2H); ^{13}C NMR (125 MHz, CD_3CN, 25 °C): $\delta = 17.5$, 65.1, 65.5, 67.7, 68.5, 70.4, 70.7, 70.8, 71.2, 71.9, 72.2, 106.4, 114.8, 125.0, 125.1, 126.7, 126.9, 129.5, 132.1, 132.2, 136.7, 137.5, 138.3, 141.0, 144.4, 146.0, 146.8, 150.2, 150.8, 154.3 ppm; MS (FAB): *m*/*z* (%): 1569 (5) $[M - PF_6]^+$, 1424 (24) $[M - 2PF_6]^+$, 1280 (14) $[M - 3PF_6]^+$.

[2]Catenane 8·4PF$_6$: Yield: 9%; m.p. 315–317 °C (decomp); ^{1}H NMR (500 MHz, CD_3COCD_3, 25 °C): $\delta = 2.20$ (s, 6H), 2.75 (d, $J = 8.1$ Hz, 2H), 3.59 (t, $J = 7.5$, 2H), 3.80–4.39 (m, 30H), 5.99 (d, $J = 5.7$, 2H), 6.02 (d, $J = 5.7$ Hz, 2H), 6.09 (d, $J = 13.8$ Hz, 2H), 6.15 (t, $J = 8.1$Hz, 2H), 6.26 (d, $J = = 13.8$ Hz, 2H), 6.33 (d, $J = 6.0$ Hz, 2H), 6.37 (d, $J = 8.0$ Hz, 2H), 6.77 (d, $J = 8.0$ Hz, 2H), 7.06 (d, $J = 6.5$ Hz, 2H), 7.13 (t, $J = 8.0$ Hz, 2H), 7.27 (d, $J = 6.7$ Hz, 2H), 7.29 (d, $J = 8.0$ Hz, 2H), 8.70 (d, $J = 6.7$ Hz, 2H), 8.91 (s, 2H), 9.31 ppm (d, $J = 6.0$ Hz, 2H); ^{13}C NMR (125 MHz, CD_3CN, 25 °C): $\delta = 16.6$, 64.6, 64.8, 67.5, 68.1, 69.5, 69.6, 69.7, 70.5, 71.0, 71.3, 104.0, 105.4, 109.2, 113.7, 122.5, 123.8, 124.2, 125.4, 125.7, 127.0, 128.4, 131.4, 136.0, 136.1, 137.4, 139.2, 142.4, 143.3, 144.5, 145.9, 148.0, 150.9, 153.3 ppm; MS (ESMS): *m*/*z* (%): 1620 $[M - PF_6]^+$.

[3]Catenane 9·4PF$_6$: Yield: 11%; m.p. 303–305 °C (decomposed); ^{1}H NMR (500 MHz, CD_3CN, 25 °C): $\delta = 1.78$ (s, 12H), 3.48–3.40 (m, 16H), 3.60–3.80 (m, 16H), 3.70–3.80 (m, 16H), 5.79 (s, 24H), 5.89 (s, 8H), 7.41 (d, $J = 6.2$ Hz, 4H), 7.72 (d, $J = 8.0$ Hz, 8H), 7.79 (d, $J = 8.0$ Hz, 16H), 8.74 (d, $J = 6.1$ Hz, 4H), 8.80 (s, 4H), 8.99 ppm (d, $J = 8.0$ Hz, 8H); ^{13}C NMR (125 MHz, CD_3CN, 25 °C): $\delta = 15.8$, 67.3, 69.5, 70.0, 70.3, 114.4, 125.1, 127.2, 130.4, 130.5, 134.3, 135.1, 137.7, 142.1, 145.5, 145.9, 151.5, 151.8 ppm; MS (ESMS): *m*/*z*: 1520 $[M - 2PF_6]^{2+}$.

[3]Catenane 10·4PF$_6$: Yield: 27%; m.p. 220–224 °C (decomposed); ^{1}H NMR (500 MHz, CD_3CN, 25 °C): $\delta = 1.35$ (s, 12H), 3.41 (s, 8H), 3.64 (s, 8H), 3.76 (s, 8H), 3.83 (s, 8H), 3.88 (s, 8H), 3.93 (s, 8H), 3.98 (s, 8H),

4.08 (s, 8H), 5.54 (s, 4H), 5.71 (s, 8H), 5.87 (s, 16H), 6.32 (dd, $J = 8.0$ Hz, 4H), 6.43 (d, $J = 8.0$ Hz, 4H), 6.94 (s, 8H), 7.27 (d, $J = 6.8$ Hz, 8H), 7.84 (d, $J = 8.2$ Hz, 8H), 7.96 (d, $J = 8.2$ Hz, 8H), 8.60 (s, 4H), 8.61 (d, $J = 6.4$ Hz, 4H), 7.27 ppm (d, $J = 6.8$ Hz, 8H); ^{13}C NMR (125 MHz, CD_3CN, 25 °C): $\delta = 15.3$, 64.0, 67.5, 67.8, 69.3, 69.6, 69.9, 70.4, 70.6, 70.7, 104.8, 111.9, 114.6, 115.7, 124.5, 124.9, 125.9, 126.7, 130.7, 130.8, 134.7, 135.5, 137.5, 141.9, 144.3, 144.6, 145.1, 151.1, 151.8, 152.7; MS (ESMS): m/z: 1570 $[M - 2PF_6]^{2+}$; elemental analysis calcd (%) for $C_{140}H_{156}F_{48}N_8O_{20}P_8$ (3430): C 47.60, H 4.60, N 3.36; found: C 47.69, H 4.71, N 3.32.

[3]Catenane 11·4PF$_6$: Yield: 24%; m.p. 249–251 °C; ^{1}H NMR (500 MHz, CD_3CN, 25 °C): $\delta = 1.30$ (s, 12H), 3.80–3.95 (s, 64H), 5.67 (s, 8H), 5.85 (s, 16H), 6.38 (d, $J = 7.6$ Hz, 8H), 6.57 (s, 16H), 6.82 (d, $J = 6.8$ Hz, 8H), 7.85 (d, $J = 8.3$ Hz, 8H), 8.00 (d, $J = 8.3$ Hz, 8H), 8.50 (s, 4H), 8.54 (d, $J = 6.2$ Hz, 4H), 8.73 ppm (br s, 8H); ^{13}C NMR (125 MHz, CD_3CN, 25 °C): $\delta = 15.1$, 67.7, 69.8, 70.6, 71.0, 105.0, 112.3, 123.8, 125.0, 125.8, 126.4, 130.8, 130.9, 134.8, 135.5, 137.3, 141.9, 143.0, 144.0, 144.8, 150.9, 152.7 ppm; MS (ESMS): m/z (%): 1620 $[M - PF_6]^+$.

X-ray crystallographic data for 6·4PF$_6$, 7·4PF$_6$, 8·4PF$_6$, 9·8PF$_6$, 10·8PF$_6$, and 11·8PF$_6$: Table 6 provides a summary of the crystallographic data for compounds **6**·4PF$_6$–**11**·8PF$_6$. Data were collected on Siemens P4/PC diffractometers by using ω-scans. The structures were solved by direct methods and they were refined based on F^2 using the SHELXTL program system.[39] Disorder was found to be present in part of either one or both of the unique polyether arms in each of structures **7**·4PF$_6$–**11**·8PF$_6$, in the position of the methyl substituents on one of the pyridinium rings of each bipyridinium unit in **10**·8PF$_6$, and of both of the methyl substituents on one of the bipyridinium units in **11**·8PF$_6$. In each case, two partial occupancy orientations were identified with the major occupancy non-hydrogen atoms being refined anisotropically and their minor occupancy counterparts refined isotropically. The absolute structure of **11**·8PF$_6$ was determined by a combination of R factor tests [$R_1^+ = 0.0781$, $R_1^- = 0.0786$] and by use of the Flack parameter [$x^+ = +0.21(10)$, $x^- = +0.79(10)$]. CCDC-191624–191628 contain the supplementary crystallographic data for this paper. These data can be obtained free of charge via www.ccdc.cam.ac.uk/conts/retrieving.html (or from the Cambridge Crystallographic Data Centre, 12 Union Road, Cambridge CB2 1EZ, UK; fax: (+44) 1223–336033; or deposit@ccdc.cam.uk).

Acknowledgement

This work is based upon research supported in part by the National Science Foundation under equipment grant CHE-9974928.

[1] J. F. Stoddart, H.-R. Tseng, *Proc. Natl. Acad. Sci.* **2002**, *99*, 4797–4800.
[2] For books and monographs on the template-directed syntheses of catenanes and rotaxanes, see: a) *Templated Organic Synthesis* (Eds.: F. Diederich, P. J. Stang), Wiley-VCH, Weinheim, **1999**; b) *Molecular Catenanes, Rotaxanes and Knots* (Eds.: J.-P. Sauvage, C. O. Dietrich-Buchecker), Wiley-VCH, Weinheim, **1999**; c) " Self-Assembly in Supramolecular Systems": L. F. Lindoy, I. M. Atkinson, in *Monographs in Supramolecular Chemistry* (Ed.: J. F. Stoddart), Royal Society of Chemistry, Cambridge, **2000**; for reviews on the template-directed syntheses of catenanes, see: d) D. Philp, J. F. Stoddart, *Synlett* **1991**, 445–458; e) J.-C. Chambron, C. O. Dietrich-Buchecker, J.-P. Sauvage, *Top. Curr. Chem.* **1993**, *165*, 131–162; f) H. W. Gibson, H. Maraud, *Adv. Mater.* **1993**, *5*, 11–21; g) D. B. Amabilino, J. F. Stoddart, *Chem. Rev.* **1995**, *95*, 2725–2828; h) D. Philp, J. F. Stoddart, *Angew. Chem.* **1996**, *108*, 1242–1286; *Angew. Chem. Int. Ed. Engl.* **1996**, *35*, 1154–1196; i) M. Fujita, K. Ogura, *Coord. Chem. Rev.* **1996**, *148*, 249–264; j) R. Jäger, F Vögtle, *Angew. Chem.* **1997**, *109*, 966–980; *Angew. Chem. Int. Ed. Engl.* **1997**, *36*, 930–944; k) G. A. Breault, C. A. Hunter, P. C. Mayers, *Tetrahedron* **1999**, *55*, 5265–5293; l) T. J. Hubin, D. H. Busch, *Coord. Chem. Rev.* **2000**, *200–202*, 5–52; m) L. Raehm, D. G. Hamilton, J. K. M. Sanders, *Synlett* **2002**, 1743–1761.
[3] D. B. Amabilino, P. R. Ashton, A. S. Reder, N. Spencer, J. F. Stoddart, *Angew. Chem.* **1994**, *106*, 1316–1320; *Angew. Chem. Int. Ed. Engl.* **1994**, *33*, 1286–1290.
[4] a) D. B. Amabilino, P. R. Ashton, S. E. Boyd, J. Y. Lee, S. Menzer, J. F. Stoddart and D. J. Williams, *Angew. Chem.* **1997**, *109*, 2160–2162; *Angew. Chem. Int. Ed. Engl.* **1997**, *36*, 2070–2072. b) D. B. Amabilino, P. R. Ashton, V. Balzani, S. E. Boyd, A. Credi, J. Y. Lee, S. Menzer, J. F. Stoddart, M. Venturi, D. J. Williams, *J. Am. Chem. Soc.* **1998**, *120*, 4295–4307.

Table 6. Crystal data, data collection and refinement parameters for compounds **6**·4PF$_6$, **7**·4PF$_6$, **8**·4PF$_6$, **9**·8PF$_6$, and **11**·8PF$_6$.[a]

	6·4PF$_6$	**7**·4PF$_6$	**8**·4PF$_6$	**9**·8PF$_6$	**11**·8PF$_6$
formula	$[C_{66}H_{76}N_4O_{10}][PF_6]_4$	$[C_{70}H_{78}N_4O_{10}][PF_6]_4$	$[C_{74}H_{80}N_4O_{10}][PF_6]_4$	$[C_{132}H_{152}N_8O_{20}][PF_6]_8$	$[C_{148}H_{160}N_8O_{20}][PF_6]_8$
solvent	6MeCN	5MeCN	8MeCN	5.5MeCN·4$C_5H_{12}O$	2$C_6H_{14}O$·6MeCN
M_r	1911.5	1920.5	2093.7	3908.8	3981.3
color, habit	red needles	red rhombs	orange rhombic needles	orange/red platy needles	orange/red blocks
crystal size [mm]	0.73 × 0.10 × 0.10	1.00 × 0.67 × 0.67	1.00 × 0.23 × 0.10	0.83 × 0.83 × 0.07	0.90 × 0.50 × 0.43
T [K]	203	193	183	183	183
crystal system	monoclinic	monoclinic	triclinic	triclinic	orthorhombic
space group	$C2/c$ (no. 15)	$P2_1/n$ (no. 14)	$P\bar{1}$ (no. 2)	$P\bar{1}$ (no. 2)	$Fdd2$ (no. 43)
a [Å]	28.804(3)	13.750(2)	13.402(2)	15.533(4)	41.317(3)
b [Å]	25.550(2)	18.156(3)	13.945(3)	15.727(6)	64.194(5)
c [Å]	13.429(2)	36.287(5)	29.060(4)	22.646(4)	14.887(1)
α [°]	90	90	87.15(1)	94.72(3)	90
β [°]	111.21(1)	98.00(1)	76.91(1)	97.93(2)	90
γ [°]	90	90	74.28(1)	117.63(2)	90
V [Å^3]	9213(2)	8971(2)	5092(2)	4786(2)	39485(5)
Z	4 [b]	4	2	1[c]	8[b]
ρ_{calcd} [g^{-1}cm^{-3}]	1.378	1.422	1.366	1.356	1.339
μ [mm^{-1}]	1.71	1.75	1.60	1.66	1.61
θ range [°]	2.4–60.0	2.5–60.0	1.6–60.0	3.2–55.0	2.5–64.0
reflections measured	6822	12623	14738	11694	8468
reflections observed [$\lvert F_o\rvert > 4\sigma(\lvert F_o\rvert)$]	4330	8997	8770	6969	6593
absorption correction	–	–	–	–	ellipsoidal
max/min transmission	–	–	–	–	0.40/0.22
parameters	619	1234	1392	1309	1359
R_1/wR_2[d]	0.068/0.166	0.077/0.195	0.099/0.258	0.108/0.283	0.078/0.210

[a] Details in common: graphite monochromated $Cu_{K\alpha}$ radiation, rotating anode source, refinement based on F^2. [b] The complex has crystallographic C_2 symmetry. [c] The complex has crystallographic C_i symmetry. [d] $R_1 = \Sigma\lvert\lvert F_o\rvert - \lvert F_c\rvert\rvert/\Sigma\lvert F_o\rvert$; $wR_2 = \{\Sigma[w(F_o^2 - F_c^2)^2]/\Sigma[w(F_o^2)^2]\}^{1/2}$; $w^{-1} = \sigma^2(F_o^2) + (aP)^2 + bP$.

[5] M. Asakawa, P. R. Ashton, S. Menzer, F. M. Raymo, J. F. Stoddart, A. J. P. White, and D. J. Williams, *Chem. Eur. J.* **1996**, *2*, 877–893.

[6] a) B. Odell, M. V. Reddington, A. M. Z. Slawin, N. Spencer, J. F. Stoddart, D. J. Williams, *Angew. Chem.* **1988**, *100*, 1605–1608; *Angew. Chem. Int. Ed. Engl.* **1988**, *27*, 1547–1550; b) M. Asakawa, W. Dehaen, G. L'abbé, S. Menzer, J. Nouwen, F. M. Raymo, J. F. Stoddart, D. J. Williams, *J. Org. Chem.* **1996**, *61*, 9591–9595.

[7] For papers and reviews on C–H···O hydrogen bonds, see: a) G. R. Desiraju, *Acc. Chem. Res.* **1991**, *24*, 290–296; b) G. R. Desiraju, *Acc. Chem. Res.* ***1996***, 29, 441–449; c) T. Steiner, *Chem. Commun.* **1996**, 727–734; d) I. Berger, M. Egli, *Chem. Eur. J.* **1997**, *3*, 1400–1404; e) K. N. Houk, S. Menzer, S. P. Newton, F. M. Raymo, J. F. Stoddart, and D. J. Williams, *J. Am. Chem. Soc.* **1999**, *121*, 1479–1487; f) F. M. Raymo, M. D. Bartberger, K. N. Houk, J. F. Stoddart, *J. Am. Chem. Soc.*, **2001**, *123*, 9264–9267; g) T. Steiner, *Angew. Chem.* **2002**, *114*, 50–80; *Angew. Chem. Int. Ed.* **2002**, *41*, 48–76; h) G. R. Desiraju, *Acc. Chem. Res.* **2002**, *35*, 565–573.

[8] For papers and reviews on π···π stacking interactions, see: a) C. A. Hunter, J. K. M. Sanders, *J. Am. Chem. Soc.* **1990**, **112**, 5525–5534; b) M. H. Schwartz, *J. Inclusion Phenom.* **1990**, *9*, 1–35; c) J. H. Williams, *Acc. Chem. Res.* **1993**, *26*, 539–598; d) C. A. Hunter, *Angew. Chem.* **1993**, *105*, 1653–1655; *Angew. Chem. Int. Ed. Engl.* **1993**, *32*, 1584–1586; e) C. A. Hunter, *J. Mol. Biol.* **1993**, *230*, 1025–1054; f) T. Dahl, *Acta. Chem. Scand.* **1994**, *48*, 95–116; g) F. Cozzi, J. S. Siegel, *Pure Appl. Chem.* **1995**, *67*, 683–689; h) C. G. Claessens, J. F. Stoddart, *J. Phys. Org. Chem.* **1997**, *10*, 254–272.

[9] For papers and reviews on C–H···π stacking interactions, see: a) M. Oki, *Acc. Chem. Res.* **1990**, *23*, 351–356; b) M. C. Etter, *J. Phys. Chem.* **1991**, *95*, 4601–4610; c) M. J. Zaworotko, *Chem. Soc. Rev.* **1994**, *23*, 282–288; d) M. Nishio, Y. Umezawa, M. Hirota, Y. Takeuchi, *Tetrahedron* **1995**, *51*, 8665–8701; e) M. Nishio, Y. Umezawa, M. Hirota, Y. Takeuchi, *The C–H···π Interaction*, Wiley-VCH, New York, **1998**; f) K. Kim, S. Paliwal, C. S. Wilcox, *J. Am. Chem. Soc.* **1998**, *120*, 11192–11193; g) H. Suezawa, T. Yoshida, M. Hirota, H. Takahashi, Y. Umezawa, K. Honda, S. Tsuboyama, M. Nishio, *J. Chem. Soc. Perkin Trans. 2* **2001**, 2053–2058; h) F. J. Carver, C. A. Hunter, D. J. Livingstone, J. F. McCabe, E. M. Seeward, *Chem. Eur. J.* **2002**, *8*, 2847–2859; i) G. Chessari, C. A. Hunter, C. M. R. Low, M. J. Packer, J. G. Vinter, C. Zonta, *Chem. Eur. J.* **2002**, *8*, 2860–2867.

[10] P. R. Ashton, R. Ballardini, V. Balzani, A. Credi, M. T. Gandolfi, S. Menzer, L. Pérez-García, L. Prodi, J. F. Stoddart, M. Venturi, A. J. P. White, D. J. Williams, *J. Am. Chem. Soc.* **1995**, *117*, 11171–11197.

[11] a) P. R. Ashton, S. E. Boyd, A. Brindle, S. J. Langford, S. Menzer, L. Pérez-García, J. A. Preece, F. M. Raymo, N. Spencer, J. F. Stoddart, A. J. P. White, D. J. Williams, *New J. Chem.* **1999**, 587–602; b) V. Balzani, A. Credi, S. J. Langford, F. M. Raymo, J. F. Stoddart, and M. Venturi, *J. Am. Chem. Soc.* **2000**, *122*, 3542–3543.

[12] a) M. Asakawa, P. R. Ashton, V. Balzani, A. Credi, C. Hamers, G. Mattersteig, M. Montalti, A. N. Shipway, N. Spencer, J. F. Stoddart, M. S. Tolley, M. Venturi, A. J. P. White, D. J. Williams, *Angew. Chem.* **1998**, *110*, 357–361; *Angew. Chem. Int. Ed.* **1998**, *37*, 333–337; b) V. Balzani, A. Credi, G. Mattersteig, O. A. Matthews, F. M. Raymo, J. F. Stoddart, M. Venturi, A. J. P. White, D. J. Williams, *J. Org. Chem.* **2000**, *65*, 1924–1936.

[13] C. L. Brown, U. Jonas, J. A. Preece, H. Ringsdorf, M. Seitz, and J. F. Stoddart, *Langmuir* **2000**, *16*, 1924–1930.

[14] M. Asakawa, M. Higuchi, G. Mattersteig, T. Nakamura, A. R. Pease, F. M. Raymo, T. Shimizu, and J. F. Stoddart, *Adv. Mater.* **2000**, *12*, 1099–1102.

[15] a) A. R. Pease, J. O. Jeppesen, J. F. Stoddart, Y. Luo, C. P. Collier, J. R. Heath, *Acc. Chem. Res.* **2001**, *34*, 433–444; b) A. R. Pease, J. F. Stoddart, *Struct. Bond.* **2001**, *99*, 189–236.

[16] a) C. P. Collier, G. Mattersteig, E. W. Wong, Y. Luo, K. Beverly, J. Sampaio, F. M. Raymo, J. F. Stoddart, J. R. Heath, *Science* **2000**, *289*, 1172–1175; b) Y. Luo, C. P. Collier, J. O. Jeppesen, K. A. Nielsen, E. DeIonno, G. Ho, J. Perkins, H.-R. Tseng, T. Yamamoto, J. F. Stoddart, J. R. Heath, *ChemPhysChem.* **2002**, *3*, 519–525.

[17] V. Balzani, A. Credi, F. M. Raymo, J. F. Stoddart, *Angew. Chem.* **2000**, *112*, 3484–3530; *Angew. Chem. Int. Ed.* **2000**, *39*, 3348–3391.

[18] P. R. Ashton, R. Ballardini, V. Balzani, A. Credi, R. Dress, E. Ishow, O. Kocian, J. A. Preece, N. Spencer, J. F. Stoddart, M. Venturi, S. Wenger, *Chem. Eur. J.* **2000**, *6*, 3558–3574.

[19] a) P. R. Ashton, M. Belohradsky, D. Philp, N. Spencer, J. F Stoddart, *J. Chem. Soc. Chem. Commun.* **1993**, 1274–1277; b) M. Asakawa, P. R. Ashton, R. Ballardini, V. Balzani, M. Belohradsky, M. T. Gandolfi, O. Kocian, L. Prodi, F. M. Raymo, J. F. Stoddart, M. Venturi, *J. Am. Chem. Soc.*, **1997**, *119*, 302–310; c) M. Händel, M. Plevoets, S. Gestermann, F. Vögtle, *Angew. Chem.* **1997**, *109*, 1248–1250; *Angew. Chem. Int. Ed. Engl.* **1997**, *36*, 1199–1201; d) F. M. Raymo, K. N. Houk, J. F. Stoddart, *J. Am. Chem. Soc.* **1998**, *120*, 9318–9322; e) M. C. T. Fyfe, F. M. Raymo, J. F. Stoddart in *Stimulating Concepts in Chemistry* (Eds.: M. Shibasaki, J. F. Stoddart, F. Vögtle), Wiley-VCH, Weinheim, 2000, pp. 211–220.

[20] a) P. R. Ashton, E. J. T. Chrystal, J. P. Mathias, K. P. Parry, A. M. Z. Slawin, N. Spencer, J. F. Stoddart, D. J. Williams, *Tetrahedron Lett.* **1987**, *28*, 6367–6370; b) D. G. Hamilton, J. E. Davies, L. Prodi, J. K. M. Sanders, *Chem. Eur. J.* **1998**, *4*, 608–620.

[21] a) P. R. Ashton, M. Blower, D. Philp, N. Spencer, J. F. Stoddart, M. S. Tolley, R. Ballardini, M. Ciano, V. Balzani, M. T. Gandolfi, L. Prodi, C. H. McLean, *New J. Chem.* **1993**, *17*, 689–695; b) P. R. Ashton, R. Ballardini, V. Balzani, A. Credi, M. T. Gandolfi, S. Menzer, L. Pérez-García, L. Prodi, J. F. Stoddart, M. Venturi, A. J. P. White, D. J. Williams, *J. Am. Chem. Soc.* **1995**, *117*, 11171–11197.

[22] a) M. Feigel, H. Kessler, D. Leibfritz, *J. Am. Chem. Soc.* **1979**, *101*, 1943–1950; b) B. E. Mann, *J. Magn. Reson.*, **1977**, *25*, 91–94.

[23] It seems not unlikely that, in $\mathbf{6}^{4+}$ and $\mathbf{7}^{4+}$, the hydroquinone ring of the crown ether macrocycle has to at least partially leave the inside of the tetracationic cyclophane to permit the phenylene rings to undergo rotation. It is not unreasonable to suppose that the various different processes are subtly interconnected in these [2]catenanes and also in $\mathbf{8}^{4+}$.

[24] a) A. Gourdon, *New. J. Chem.*, **1992**, *16*, 953–957; b) H. E. Zimmerman, D. S. Crumrine, *J. Am. Chem. Soc.* **1972**, *94*, 498–506.

[25] The other circumrotational process—that of the tetracationic cyclophane component through the crown ether macrocycle—is not observable by dynamic ^{1}H NMR spectroscopy since only one of the two translational isomers, that is, the one with the bipyridinium unit located inside the crown ether macrocycle, is populated.

[26] P. R. Ashton, J. A. Preece, J. F. Stoddart, M. S. Tolley, A. J. P. White, D. J. Williams, *Synthesis*, **1994**, 1344–1352.

[27] a) R. S. Cahn, C. K. Ingold, V. Prelog, *Angew. Chem.* **1966**, *78*, 413–443; *Angew. Chem. Int. Ed. Engl.* **1966**, *5*, 385–415; b) IUPAC 1974 Recommendations for Section E, "Fundamental Stereochemistry": *Pure Appl. Chem.* **1976**, *45*, 13–30; c) V. Prelog, G. Helmchen, *Angew. Chem.* **1982**, *94*, 614–630; *Angew. Chem. Int. Ed. Engl.* **1982**, *21*, 567–583; d) E. L. Eliel, S. H. Wilen, *Stereochemistry of Organic Compounds*, Wiley, New York, **1994**, Chapter 14.

[28] E. Alcalde, L. Pérez-García, S. Ramos, J. F. Stoddart, S. A. Vignon, A. J. P. White, D. J. Williams, unpublished results.

[29] a) S. J. Rowan, S. J. Cantrill, G. R. L. Cousins, J. K. M. Sanders, J. F. Stoddart, *Angew. Chem.* **2002**, *114*, 938–993; *Angew. Chem. Int. Ed.* **2002**, *41*, 898–952; b) S. Otto, R. L. E. Furlan, J. K. M. Sanders, *Science* **2002**, *297*, 590–593.

[30] Examination of the isomerization processes in Figures 12–14 reveals a similarity with the phenomenon of residual stereoisomerism (P. Finocchiaro, D. Gust, K. Mislow, *J. Am. Chem. Soc.* **1974**, *96*, 3198–3205). For example, the rapid interconversion (Process I) between the diastereomeric pairs (*aS*)-(*P*) and (*aS*)-(*M*), and (*aR*)-(*P*) and (*aR*)-(*M*) results in apparent loss of the helical chirality, leading to residual enantiomerism where the two enantiomers have only axial chirality.

[31] It should be recalled that the separation between two peaks in Hz is directly proportional to the exchange rate required for coalescence to occur.

[32] A similar determination of the diastereoisomeric ratio present in $\mathbf{7}\cdot 4PF_6$ in CD_3COCD_3 at low temperatures was prevented by overlapping signals in the region of the ^{1}H NMR spectrum associated with the minor diastereoisomer of that [2]catenane.

[33] The starting geometries for the two diastereoisomers were constructed from the X-ray crystal structure and input into Macromodel 5.0 (F. Mohamadi, N. G. J. Richards, R. Liskamp, M. Lipton, C. Caulfield, G. Chang, T. Hendrickson, W. C. Still, *J. Comput. Chem.* **1990**, *11*, 440–467). Each geometry was then subjected to a Monte Carlo conformational search of 4000 conformers followed by energy minimization. The AMBER* force field with the GB/SA $CHCl_3$ solvent model was used.

[34] D. D. Perrin, W. F. L. Armarego, *Purification of Laboratory Chemicals*, Pergamon Press, Oxford, **1989**.
[35] J. Rebek, Jr., T. Costello, R. Wattley, *J. Am. Chem. Soc.* **1985**, *107*, 7487–7493.
[36] P.-L. Anelli, P. R. Ashton, R. Ballardini, V. Balzani, M. Delgado, M. T. Gandolfi, T. T. Goodnow, A. E. Kaifer, D. Philp, M. Pietraszkiewicz, L. Prodi, M. V. Reddington, A. M. Z. Slawin, N. Spencer, J. F. Stoddart, C. Vicent, D. J. Williams, *J. Am. Chem. Soc.* **1992**, *114*, 193–218.
[37] A. L. Van Geet, *Anal. Chem.* **1970**, *42*, 679–680.
[38] Spinworks Version 1.3, K. Marat, Department of Chemistry, University of Manitoba (Canada).
[39] a) SHELXTL PC Version 5.03, Siemens Analytical X-Ray Instruments, Madison, WI, **1994**; b) SHELXTL PC Version 5.1, Bruker AXS, Madison, WI, **1997**.

Received: August 28, 2002 [F4376]

  0947-6539/03/0902-0556 $ 20.00+.50/0